

Kuraganti Vasu<sup>a,b</sup>, Mangalampalli Sri Rama Narasimha Kiran<sup>a,c</sup>,  
Mamidipudi Ghanashyam Krishna<sup>a,b</sup>, Kuppuswamy Anantha Padmanabhan<sup>b,d</sup>

<sup>a</sup>School of Physics, University of Hyderabad, Hyderabad, India

<sup>b</sup>Centre for Nanotechnology, University of Hyderabad, Hyderabad, India

<sup>c</sup>Department of Electronic Materials Engineering, Research School of Physics and Engineering,  
The Australian National University, Canberra, Australia

<sup>d</sup>School of Engineering Sciences and Technology, University of Hyderabad, Hyderabad, India

# Nitrogen deficiency and metal dopant induced sub-stoichiometry in titanium nitride thin films: a comparative study

*This paper is dedicated to our friend and colleague, Prof. Horst Hahn, who celebrated his 60<sup>th</sup> birthday recently*

Sub-stoichiometric (nitrogen-deficient) and Nb-substituted ( $\text{Ti}_{1-y}\text{Nb}_y\text{N}$ ,  $0 \leq y \leq 1$ ) titanium nitride thin films were deposited by means of radio frequency magnetron sputtering on  $\text{SiO}_2$  and Si (311) substrates and compared. Thickness of  $\text{TiN}_x$  films varied in the range 116–230 nm, while the value was constant, at 500 nm, for  $\text{Ti}_{1-y}\text{Nb}_y\text{N}$  films. The sub-stoichiometric  $\text{TiN}_x$  films deposited at room temperature are amorphous, independent of nitrogen partial pressure (in the range of 1.6 to 3.33 Pa). Annealing of the films at 600 °C resulted in amorphous–crystalline transition only in the film deposited at 3.33 Pa, which crystallized into tetragonal  $\epsilon\text{-Ti}_2\text{N}$  phase. The other films remained amorphous. The hardness and Young's modulus were highest for the film deposited at a nitrogen pressure of 3.33 Pa, viz., 5.9 GPa and 105 GPa respectively. In contrast, all as-deposited Nb substituted  $\text{TiN}$  ( $\text{Ti}_{1-y}\text{Nb}_y\text{N}$ ) films crystallized into rock salt structure with (111) orientation up to  $y = 0.77$ . The hardness and Young's modulus for  $\text{Ti}_{1-y}\text{Nb}_y\text{N}$  films increased with increase in Nb concentration. The highest values of hardness and Young's modulus obtained were 29 GPa and 320 GPa respectively. This study shows that nitrogen deficient titanium nitrides are more difficult to crystallize and exhibit lower hardness than metal substituted nitrides.

**Keywords:** Magnetron sputtering; Non-stoichiometric compounds; Nitrides of titanium; anion deficiency; cation substitution

## 1. Introduction

TiN is regarded as a prototype transition-metal nitride system [1] that exhibits a unique combination of properties such as high hardness, wear resistance, melting point, electrical conductivity, good chemical inertness and gold-like color. It is, therefore, widely used in a variety of applica-

tions encompassing semiconductor, decorative and tribological coating industries. For example, thin films of TiN are used very successfully as interconnector and diffusion barriers in ULSI circuits [2–6]. These applications rely mainly on the properties stoichiometric ( $[\text{N}]/[\text{Ti}] \approx 1$ ) and cubic TiN films. There are a number of nitrogen deficient sub-stoichiometric ( $[\text{N}]/[\text{Ti}] \neq 1$ ) forms of TiN with properties that are very different from those of the stoichiometric phase. The major source of non-stoichiometry in  $\text{TiN}_x$  thin film is anion vacancies for  $x < 1$  and interstitial N atoms for  $x > 1$  [7], where the cation vacancies are present at the Ti sub lattice. A challenge in this area is to realize single phase sub-stoichiometric  $\text{TiN}_x$  films to enable exploitation of their unique properties. In the case of reactively sputtered TiN film, the variation of nitrogen partial pressure during deposition is used to realize sub-stoichiometric phases [8]. Another approach to induce non-stoichiometry in titanium nitride is incorporation of additional transition metal (*Me*) into TiN. This leads to the formation of a ternary nitride ( $\text{Ti}_{1-y}\text{Me}_y\text{N}$ ) with improved physical and chemical properties [9]. The metal substitution strongly affects the crystal structure, chemical bonding, electronic structure and free electron concentration, which, in turn, significantly modify the structural, mechanical, electrical and optical properties.

To the best of our knowledge, a comparative study of variations in properties of nitrogen deficiency and metal dopant induced sub-stoichiometry in titanium nitride thin films has not been reported previously. In this study both sub-stoichiometric and metal-substituted titanium nitride thin films are deposited using radio frequency (RF) magnetron sputtering on  $\text{SiO}_2$  and Si substrates in 100 % nitrogen atmosphere. The composition of sub-stoichiometric TiN is controlled by varying the nitrogen partial pressure and Nb-substituted TiN films by varying the Nb concentration in the cathode. The growth, microstructure, structure and nanomechanical properties of these two systems are studied and compared.

## 2. Experimental

Sub-stoichiometric  $\text{TiN}_x$  and  $\text{Ti}_{1-y}\text{Nb}_y\text{N}$ ,  $0 \leq y \leq 1$ , films were deposited using RF magnetron sputtering on  $\text{SiO}_2$  and Si (311) substrate. The composition was controlled by varying the nitrogen partial pressure and Nb concentration in sub-stoichiometric  $\text{TiN}_x$  and  $\text{Ti}_{1-y}\text{Nb}_y\text{N}$  films respectively. The  $\text{SiO}_2$  and Si substrates were clamped to the substrate holder and the distance between the target and the substrate was maintained at 5 cm. After achieving the ultimate vacuum, i.e.  $3 \times 10^{-4}$  Pa, the chamber was filled with pure nitrogen gas up to required working gas pressures. The RF power was maintained at 60 and 100 W for the deposition of  $\text{TiN}_x$  and  $\text{Ti}_{1-y}\text{Nb}_y\text{N}$  films respectively.  $\text{TiN}_x$  films were deposited at room temperature and  $\text{Ti}_{1-y}\text{Nb}_y\text{N}$  was deposited at a substrate temperature of  $250^\circ\text{C}$ . Sub-stoichiometric  $\text{TiN}_x$  films are subjected to post deposition rapid thermal annealing for 1 min at a temperature of  $600^\circ\text{C}$ . Before introducing nitrogen gas, the target was pre-sputtered for 15 min in the presence of argon gas. The deposition time for all films was 2 h. Prior to deposition, the substrates were cleaned by rinsing in ultrasonic bath of acetone, iso-propanol and deionized water, followed by ion bombardment in argon plasma for 8 min.

The thickness of the films was determined by using a surface profilometer (Model XP-1, Ambios Technology, USA). The crystal structures of  $\text{TiN}_x$  and  $\text{Ti}_{1-y}\text{Nb}_y\text{N}$  films were determined using a wide-angled powder X-ray diffractometer (XRD) equipped with a position-sensitive detector. For  $\text{TiN}_x$  films  $\text{Cu-K}\alpha$  ( $\lambda = 1.5418 \text{ \AA}$ ) radiation was used to obtain the XRD pattern and for  $\text{Ti}_{1-y}\text{Nb}_y\text{N}$  films  $\text{Co-K}\alpha$  ( $\lambda = 1.7889 \text{ \AA}$ ) was used. Microstructure of the films was determined using contact mode atomic force microscopy (AFM, Seiko Inst, SPA-400, Japan). Chemical composition of the films was determined using energy-dispersive X-ray spectroscopy (EDX) analysis. Nanomechanical properties, i.e., hardness and Young's modulus of the films were determined using the nanoindentation technique (Hysitron triboindenter-900, USA). The films were indented with a Berkovich-type pyramidal diamond tip with a maximum load of  $2000 \mu\text{N}$ . The trapezoid load function (which includes the loading, holding and unloading segments) was used to measure the hardness of the films with a loading rate of  $200 \mu\text{N s}^{-1}$  and segment time of 10 s for each segment.

## 3. Results and discussion

Contact mode AFM images of  $\text{TiN}_x$  films annealed at  $600^\circ\text{C}$  are shown in Fig. 1. The film deposited at 1.6 Pa has a grain size  $36 \pm 2 \text{ nm}$  (Fig. 1a), looks less dense but continuous. Films deposited at 2.0 and 2.66 Pa (Fig. 1b and c) showed a highly dense microstructure and the shapes as well as the distributions of the particles were quite uniform. The grain sizes of these films were  $38 \pm 3$  and  $41 \pm 3 \text{ nm}$  respectively. The 3.33 Pa film (Fig. 1d) consists of larger particles that are of an average size of  $44 \pm 4 \text{ nm}$ . The average particle size increases very marginally with increasing working gas pressure, whereas root mean square roughness shows an initial increase to  $2.2 \text{ nm}$ , but then decreases to  $0.55 \text{ nm}$ . Due to the reduced thickness after annealing (due to shrinkage caused by a reduction in porosity), the microstructure is not very dense and the film is

not quite uniform, but interestingly the roughness of the film is quite low at 3.33 Pa, compared with 1.6, 2.0 and 2.66 Pa films. In all the cases there appears to be a migration of particles towards the upper surface of the film, as indicated by the white colored particles in the micrographs. The magnitude of the re-densification of the microstructure and the consequent volume change are evidently dependent on the microstructure of the as-deposited films. The films deposited at 1.60 and 3.33 Pa were less dense than those deposited at 2.0 and 2.66 Pa, and were, therefore, more drastically affected by the annealing process. At higher pressures, the energetic nitrogen particles bombard the film surface with higher kinetic energies providing sufficient energy for adatom mobility and therefore the films have higher packing density and more uniform grain size distribution.

AFM images of  $\text{Ti}_{1-y}\text{Nb}_y\text{N}$  thin films with various  $y$  values are shown in Fig. 2. From the figure, it is evident that the surface of the films consists of spherical grains with uniform size distribution. All the films exhibit dense microstructures and less porosity. The grain size of TiN films, for  $y = 0$  is  $36 \pm 4 \text{ nm}$  and for  $y = 0.26$  is  $46 \pm 5 \text{ nm}$  and finally the value increased to  $79 \pm 9 \text{ nm}$  for  $y = 0.77$ . Interestingly, the grain size of NbN film for  $y = 1$  is decreased to  $45 \pm 3 \text{ nm}$ . It is observed that the Nb concentration strongly affects the microstructure and growth of the film. In the sputtering process, the sputtering yield is dependent on the process parameters and the density of the target material. The increase in grain size with Nb concentration could be attributed to the increase in sputtering yield when Nb is substituted by Ti. Variation in root mean square roughness follows the same trend as grain size, it increased from 0.5 to 3.8 nm as  $y$  increased from 0 to 0.77 and then decreased to 3 nm for corresponding NbN film ( $y = 1$ ). The complete microstructural analysis of  $\text{TiN}_x$  and  $\text{Ti}_{1-y}\text{Nb}_y\text{N}$  films is presented in Table 1.

X-ray diffraction studies of  $\text{TiN}_x$  films deposited for different nitrogen partial pressures (1.6, 2.0, 2.66 and 3.3 Pa)

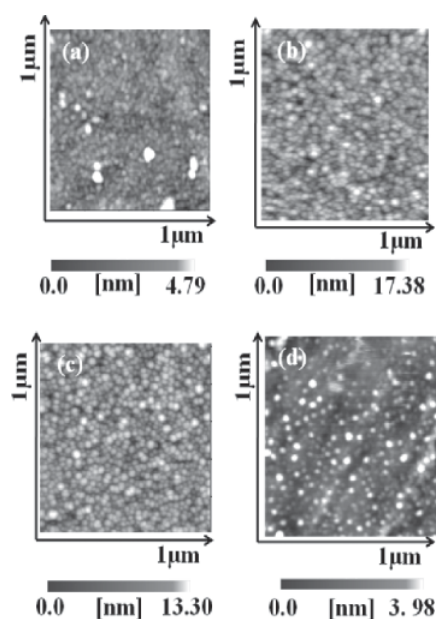


Fig. 1. Contact mode atomic force microscopy images of post deposition annealed ( $600^\circ\text{C}$ )  $\text{TiN}_x$  thin films deposited at different nitrogen partial pressures; (a) 1.6, (b) 2.0, (c) 2.66 and (d) 3.3 Pa.

at room temperature revealed that the as-deposited films did not crystallize but displayed an amorphous nature. It is known that stoichiometric TiN films crystallize either at high deposition temperatures or at high post-deposition annealing temperatures [10, 11]. All TiN<sub>x</sub> films were subjected to post-deposition annealing at 600 °C for 1 min. On annealing, the film deposited at 3.3 Pa crystallized in to tetragonal Ti<sub>2</sub>N phase and exhibited a peak corresponding to (311) orientation. The XRD pattern of annealed Ti<sub>2</sub>N deposited at 3.3 Pa is shown in Fig. 3. The films deposited at lower pressures (1.6, 2.0 and 2.66 Pa) did not crystallize even at this annealing temperature. In earlier work, the current authors have shown that there is a shift in the reflectance minimum of TiN<sub>x</sub> films as a function of nitrogen partial pressure, which was correlated with nitrogen non-stoichiometry. The minimum occurs at 2.33 eV for stoichiometric TiN, whereas in the presence of nitrogen non-stoichiometry this peak shifts to higher energies [12]. Therefore, it is inferred, in the present case also, that the films deposited at low nitrogen partial pressure are sub-stoichiometric and nitrogen deficient. The crystallite size calculated from the full width at half maximum of the peak was 60 nm.

When N is added to Ti, Ti transforms from the hexagonal closed packed (hcp) phase to the tetragonal ε-Ti<sub>2</sub>N phase, and finally to the fcc δ-TiN phase. There are several theories for the formation and stability of the Ti<sub>2</sub>N phase [13, 14]. According to Yasuhiro et al. [13], the Ti–N compound exists as a distorted α phase of a solid solution Ti–N<sub>x</sub> in the

range of  $x \leq 0.2$ , where nitrogen atoms occupy the interstitial octahedral sites in a random manner. At higher values of  $x$ ,  $0.2 < x < 0.49$ , a two-phase compound comprising the α-Ti–N<sub>x</sub> and ε-Ti<sub>2</sub>N is formed, and over a relatively narrow range,  $0.49 \leq x \leq 0.52$ , the ε-Ti<sub>2</sub>N is stable and phase pure. At still higher nitrogen contents,  $0.52 \leq x \leq 0.60$ , ε-Ti<sub>2</sub>N is contaminated by the δ-TiN<sub>x</sub> fcc phase. At  $x = 0.6$ , the crystal structure transforms to fcc, and only δ-TiN<sub>x</sub> is present above  $x = 0.6$ . Therefore, titanium nitrides containing ε-Ti<sub>2</sub>N are usually prepared as mixed multiphase materials, and it is difficult to prepare the monophasic ε-Ti<sub>2</sub>N films via a physical vapor deposition route. The high temperature stability of the sub-stoichiometric phases such as Ti<sub>2</sub>N is due to the fact that the Ti lattice is able to accept small amounts of nitrogen at octahedral sites.

The XRD patterns of Ti<sub>1-y</sub>Nb<sub>y</sub>N films for different values of  $y$  are shown in Fig. 4. It is evident from the figure that the film for  $y = 0$  crystallized in the rock salt structure and exhibits a peak corresponding to the (111) plane of cubic TiN at  $2\theta = 43.0^\circ$ . The intensity of the reflection from the (111) plane increased for  $y = 0.26$  and it was also accompanied by a shift in the peak position to a lower diffraction angle. At higher Nb concentrations in the films, i.e. for  $y = 0.41, 0.58$  and  $0.77$ , the intensity of the reflection from the (111) plane continued to increase, with the  $2\theta$  position progressively shifting to lower diffraction angles. The shift in position of the (111) plane is attributed to an increase in the concentration of Nb into the Ti lattice sites of the structure. When Ti atoms are replaced by Nb atoms, the crystal lattice undergoes a distortion, since the radius of the Ti atom is smaller than that of the Nb atom [15]. Moreover,

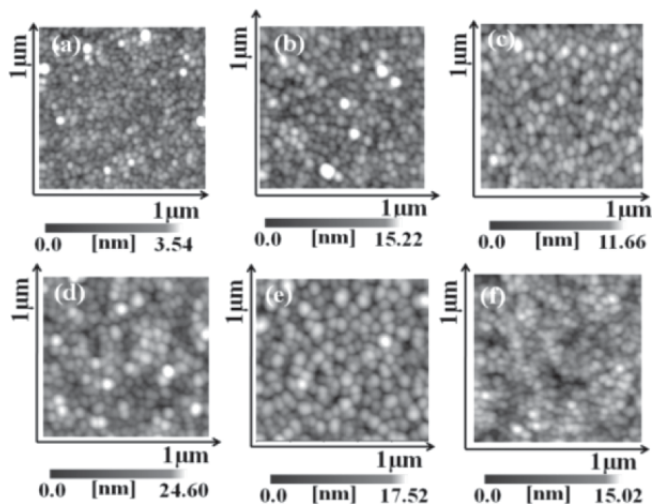


Fig. 2. Contact mode atomic force microscopy images of Ti<sub>1-y</sub>Nb<sub>y</sub>N films for different values of Nb concentration; (a)  $y = 0$ , (b)  $y = 0.26$ , (c)  $y = 0.41$ , (d)  $y = 0.58$ , (e)  $y = 0.77$  (f),  $y = 1$ .

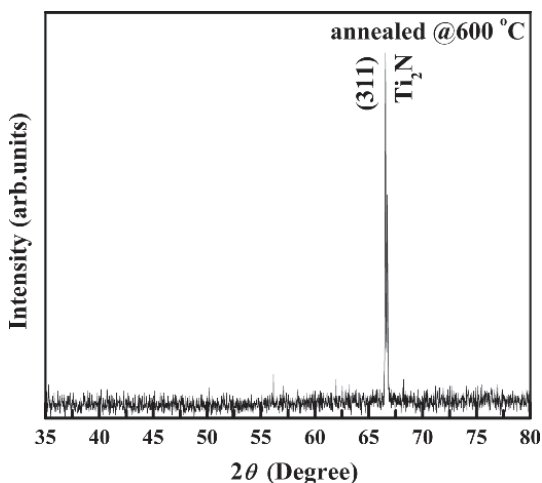


Fig. 3. XRD pattern of TiN<sub>x</sub> film deposited at 3.33 Pa after annealing at 600 °C for one minute.

Table 1. Microstructural analysis of TiN<sub>x</sub> and Ti<sub>1-y</sub>Nb<sub>y</sub>N thin films.

	TiN <sub>x</sub> films annealed @ 600 °C				Ti <sub>1-y</sub> Nb <sub>y</sub> N films					
	Nitrogen partial pressure (Pa)				Nb composition (y)					
	1.6	2.0	2.66	3.33	0	0.26	0.41	0.58	0.77	1
Grain size (nm)	36 ± 2	38 ± 3	41 ± 3	44 ± 4	36 ± 4	46 ± 5	52 ± 5	63 ± 6	79 ± 8	45 ± 3
Roughness (nm)	1.3	2.7	2.2	0.78	0.5	1	1.8	2.7	3.8	3

the difference in the atomic sizes of Ti and Nb atoms gives rise to an internal stress/strain in the film. It is known that the TiN–NbN system is miscible and the compound (Ti,Nb)N is a stable pseudo-binary alloy [15]. The NbN film for  $y = 1$  exhibits a very broad peak at  $2\theta = 36.73^\circ$  indicating the amorphous nature of NbN film. Structural study of  $\text{Ti}_{1-y}\text{Nb}_y\text{N}$  films on Si substrate is in very good agreement with our previous study on stainless steel substrate [16]. The lattice parameter of the films was calculated from XRD analysis and the value increased from 0.423 to 0.435 nm as the  $y$  value increased from 0 to 0.77. The stabilization of ternary  $\text{Ti}_{1-y}\text{Nb}_y\text{N}$  solid solution in rock salt structure indicates that the substituted Nb is completely soluble in TiN up to  $y = 0.77$ .

The hardness ( $H$ ) and Young's modulus ( $E$ ) of  $\text{TiN}_x$  and  $\text{Ti}_{1-y}\text{Nb}_y\text{N}$  films were calculated from the load–displacement curves using the Oliver–Pharr analysis [17]. The hardness of  $\text{TiN}_x$  films as a function of normalized depth for different working gas pressures is presented in Fig. 5a and b. The hardness decreases with decreasing nitrogen pressure and reaches a minimum value at 1.6 Pa. To determine the “film only hardness” from the composite hardness (substrate + film), the data were fitted using the Korsunsky model [18], using the equation

$$H_c = H_s + [(H_f - H_s)/1 + k\beta^2] \quad (1)$$

where  $H_c$  is the composite hardness obtained from the indentation experiment,  $H_s$  the substrate hardness, is taken as equal to 10 GPa for the quartz substrate based on our earlier indentation experiments,  $H_f$  is the film-only hardness obtained from the fit,  $k$  is a constant related to film thickness and  $\beta$  is the normalized depth, i. e., contact depth/film thickness. It can be seen from Fig. 5a that the film-only hardness for the film deposited at 1.60 Pa was 3.34 GPa, which increased to 5.9 GPa for the film deposited at 3.33 Pa. Buckle et al. [19] presented another model for determining the film only hardness. According to them, the contribution of the substrate to the composite hardness starts to become effective before the indenter crosses the film thickness completely. In this model

$$H_c = H_s + (H_f - H_s)\exp(-k\beta^n) \quad (2)$$

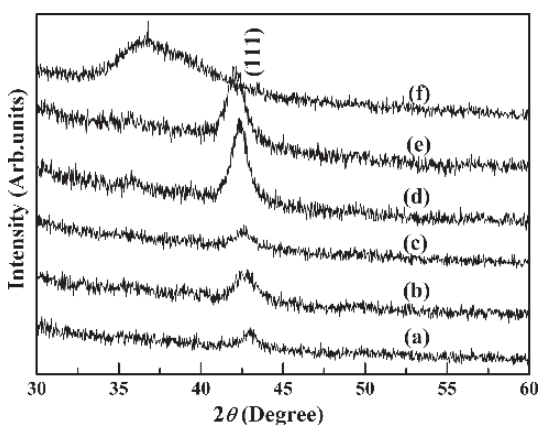


Fig. 4. XRD pattern of  $\text{Ti}_{1-y}\text{Nb}_y\text{N}$  films for different values of  $y$ . (a)  $y = 0$ ; (b)  $y = 0.26$ ; (c)  $y = 0.41$ ; (d)  $y = 0.58$ ; (e)  $y = 0.77$ ; (f)  $y = 1.00$ .

Where  $H_c$  is the composite hardness,  $H_s$  the substrate hardness,  $H_f$  the film-only hardness,  $\beta$  the relative indentation depth (i. e., normalized depth) and  $k$  and  $n$  are material parameters that characterize the change in hardness as the indenter passes from the film to the substrate.

The film-only hardness according to this model varied from 3.51 to 5.78 GPa, as the deposition pressure increased from 1.6 to 3.33 Pa (Fig. 5b). It is very interesting to note that both the models lead to similar values for the film-only hardness. The “film only hardness” of  $\epsilon\text{-Ti}_2\text{N}$  film deposited at 3.3 Pa and annealed at  $600^\circ\text{C}$  was 5.78 GPa. Chawla et al. [20] have also performed a systematic study on the effect of film thickness on the hardness of stoichiometric TiN films on glass substrates deposited at a substrate temperature of  $500^\circ\text{C}$ . They have reported hardness of 10 GPa and 100 GPa Young's modulus for the well crystallized stoichiometric TiN film with a thickness of around 200 nm. At  $2\ \mu\text{m}$  film thickness, the hardness value reached 24 GPa with a Young's modulus of 240 GPa. In contrast, the maximum value of hardness observed for  $\text{Ti}_2\text{N}$  in the present experiments is 5.9 GPa with a film thickness of 200 nm. Evidently, the difference in hardness is a result of the difference in the composition. It was not possible for us to deposit film with thickness  $> 200$  nm since beyond this thickness the film transformed from  $\epsilon\text{-Ti}_2\text{N}$  to stoichiometric TiN.

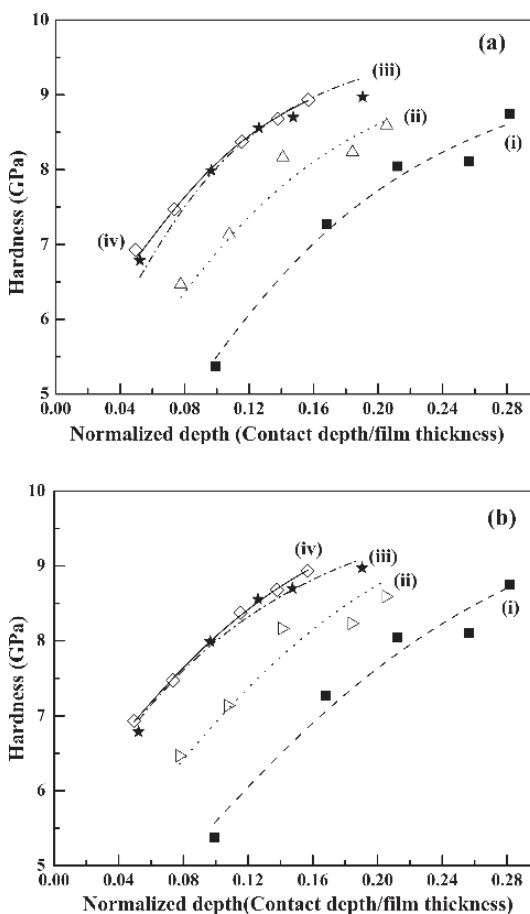


Fig. 5. Indentation hardness fitted with (a) Korsunsky model, and (b) Buckle model for determining the film-only hardness of  $\text{TiN}_x$  films deposited at different nitrogen partial pressures, with (i) 1.6 (ii) 2.0 (iii) 2.66 and (iv) 3.3 Pa.

The normalized depth vs Young's modulus ( $E$ ) is shown in Fig. 6. Similar to the hardness, Young's modulus also varies with film deposition pressure and indenter penetration into the sample. It is concluded that at depths greater than 30 nm, the Young's modulus is a composite value, with contributions from both the substrate and the film. At still higher penetration depths, the value of the Young's modulus of the film decreases towards that of the substrate (69.6 GPa for quartz). The film deposited at 3.33 Pa had the highest  $E$  value, and equaled 105 GPa, while it was equal to 76 GPa for a film deposited at 1.6 Pa. It is known that the grain size, film orientation, surface roughness, degree of porosity and the amorphous to nanocrystalline transformation all affect not only the  $H$  but also the  $E$  value of thin films. The grain size variation in this study was too small for any meaningful conclusions to be drawn on the effect of grain size on the hardness and the measured values. This effect and those of the other variables listed above will be identified in a future investigation.

The values of hardness and Young's modulus of the  $Ti_{1-y}Nb_yN$  thin films with increasing concentrations of Nb in TiN are displayed in Fig. 7. The data reveal that the hardness of the TiN film, for  $y = 0$ , is  $15 \pm 1.5$  GPa. The hardness increases with increasing Nb content and attains a maximum value of  $29 \pm 2.4$  GPa for  $y = 0.77$ . For  $y = 1$ , the hardness decreases to  $17 \pm 1.9$  GPa for the amorphous NbN film. Similar behavior is observed in the

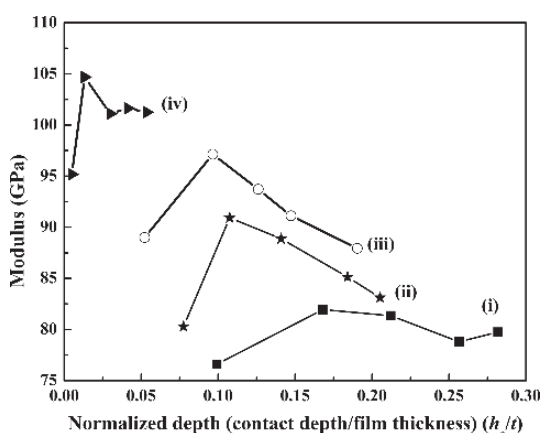


Fig. 6. Young's modulus vs. normalized depth of  $TiN_x$  films deposited at different gas pressures; (i) 1.6 (ii) 2.0 (iii) 2.66 and (iv) 3.3 Pa.

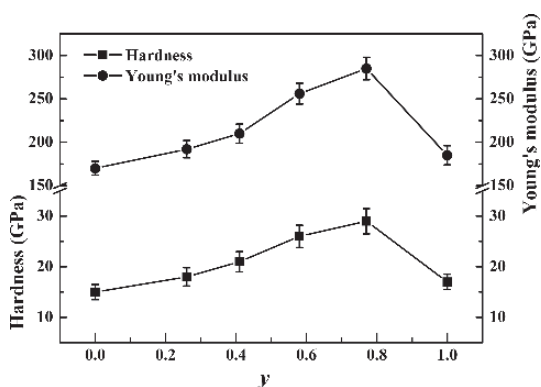


Fig. 7. Variation of hardness and Young's modulus of  $Ti_{1-y}Nb_yN$  films for different values of  $y$ .

variation of Young's modulus with the Nb content. It increased from  $175 \pm 8$  GPa to  $285 \pm 13$  GPa as  $y$  increased from 0 to 0.77 (in the cubic structure) and then reduced to  $185 \pm 11$  GPa for  $y = 1$  corresponding to the amorphous NbN film.

It is reported that the high hardness in the transition metal nitrides is due to a favorable occupancy of the hybridized Ti 3d( $e_g$ ) and N2p states leading to the covalent character [21, 22]. The bonding–antibonding valence band distribution of the N2p– $Md$  (where  $M$  is the transition metal) develops symmetrically below and above the hybridization gap. The trigonal prismatic coordination is emphasized through the strong p–d orbital mixing. In TiN, the additional valence electrons contributed by nitrogen fill the antibonding Ti3d( $e_g$ ) and 2p hybridized states at the zone center. Interestingly, the extra nitrogen electrons also populate some of the Ti3d( $t_{2g}$ ) states that build bonds between the Ti atoms. The binding energy of the nitrogen valence and core states decreases, whereas the binding energy of the cation states increases. The difference in the binding energies between corresponding anion and cation like states can be considered as a measure of the charge transfer and of the ionic/covalent character of the compound [23].

A comparison of sub-stoichiometry induced by anion deficiency and that due to metal substitution in the Ti sites clearly indicates that the nitrogen deficient  $TiN_x$  films have lower hardness than the  $Ti_{1-y}Nb_yN$  films. Evidently the covalent bonding between the metal and nitrogen is enhanced when Nb is substituted leading to higher hardness. It is significant that the materials retain the cubic structure. Similar observations have also been made in other transition metal substituted titanium nitride films. Anion deficiency, in contrast, leads to a structural phase transformation from cubic to the tetragonal structure resulting in weakening of the covalent bonds and consequently lower hardness. It has been shown previously [12, 24–26] by the present authors that a further consequence of the anion deficiency is that the films become transparent in the visible region of the spectrum with a large band gap and semiconducting nature. The Nb substituted films, however, retain the conductivity and show a peak in optical absorption in the visible region of the spectrum corresponding to the existence of a plasmon resonance [27].

#### 4. Conclusions

A comparison study of the growth, structure, microstructure and nanomechanical behavior of sub-stoichiometric TiN films is presented. Sub-stoichiometry was induced by two means; in one case by causing nitrogen deficiency leading to the formation of  $Ti_2N$  films and in the other case substituting Ti with Nb ions leading to  $Ti_{1-y}Nb_yN$ , ( $0 \leq y \leq 1$ ) films. Nitrogen deficiency results in amorphization and low hardness, while Nb substitution enhances the hardness without affecting the crystal structure. The present study demonstrates the ability to tailor the physical behavior of TiN either by anion deficiency or metal substitution.

The authors acknowledge the support received from the UPE and UGC-CAS programs. KV thanks the DST-CFN project for financial support in the form of a fellowship. MSRKN acknowledges the Dr.

DS Kothari fellowship of the UGC, Govt. of India. Infrastructural support provided by DST under the Centre for Nanotechnology, University of Hyderabad is acknowledged.

## References

- [1] L. Tsetseris, N. Kalfagiannis, S. Logothetidis, S.T. Pantelides: *Phys. Rev. Lett.* 99 (2007) 125503. PMID:17930516; DOI:10.1103/PhysRevLett.99.125503
- [2] L.A. Rocha, E. Ariza, J. Ferreira, F. Vaz, E. Ribeiro, L. Rebouta, E. Alves, A.R. Ramos, Ph. Goudeau, J.P. Riviere: *Surf. Coat. Technol.* 180–181 (2004) 158. DOI:10.1016/j.surfcoat.2003.10.059
- [3] R. Banerjee, R. Chandra, P. Ayyub: *Thin Solid Films* 405 (2002) 64. DOI:10.1016/S0040-6090(01)01705-9
- [4] P. Patsalas, S. Logothetidis: *J. Appl. Phys.* 90 (2001) 4725. DOI:10.1063/1.1403677
- [5] J.S. Chun, I. Petrov, J.E. Greene: *J. Appl. Phys.* 86 (1999) 3633. DOI:10.1063/1.371271
- [6] P. Patsalas, C. Charitidis, S. Logothetidis, C.A. Dimitriadis, O. Valassiades: *J. Appl. Phys.* 86 (1999) 5296. DOI:10.1063/1.371514
- [7] C.S. Shin, S. Rudenja, D. Gall, N. Hellgren, T.Y. Lee, I. Petrov, J.E. Greene: *J. Appl. Phys.* 95 (2004) 356. DOI:10.1063/1.1629155
- [8] H. C. Barshilia, K.S. Rajam: *Bull. Mater. Sci.* 27 (2004) 35. DOI:10.1007/BF02708482
- [9] G.M. Matenoglou, L.E. Koutsokeras, Ch.E. Lekka, G. Abadias, C. Kosmidis, G.A. Evangelakis, P. Patsalas: *Surf. Coat. Technol.* 204 (2009) 911. DOI:10.1016/j.surfcoat.2009.06.032
- [10] H.T. Kim, C.S. Chae, D.H. Han, D.K. Park: *J. Korean Phys. Soc.* 37 (2000) 319.
- [11] K. Khojier, A.A. Banimahd, H.Savaloni: *J. Theor. Appl. Phys.* 5 (2011) 25.
- [12] M.S.R.N. Kiran, M.G. Krishna, K.A. Padmanabhan: *Int. J. Nanomanufacturing*, 2 (2008) 420.
- [13] Y. Igasaki, H. Mitsuhashi: *J. Appl. Phys.* 68 (1990) 2439. DOI:10.1063/1.347175
- [14] R. Eibler: *J. Phys. Condens. Matter.* 10 (1998) 10223. DOI:10.1088/0953-8984/10/45/010
- [15] C. Engstrom, J. Birch, L. Hultman, C. Lavoie, C. Cabral, J.L.J. Sweet, J.R.A. Carlsson: *J. Vac. Sci. Technol. A* 17 (1999) 2920. DOI:10.1116/1.581961
- [16] K. Vasu, M.G. Krishna, K.A. Padmanabhan: *J. Mater. Sci.* 47 (2012) 3522. DOI:10.1007/s10853-011-6197-x
- [17] W.C. Oliver, G.M. Pharr: *J. Mater. Res.* 7 (1992), 1564. DOI:10.1557/JMR.1992.1564
- [18] A.M. Korsunsky, M.R. Mc Gurk, S.J. Bull, T.F. Page: *Surf. Coat. Technol.* 99 (1998) 171. DOI:10.1016/S0257-8972(97)00522-7
- [19] H. Buckle in: J.W. Westbrook and H. Conrad, (Eds.), *The Science of Hardness Testing and its Research Applications*, American Society for Metals, Metals Park, OH (1973) 453.
- [20] V. Chawla, R. Jayaganthan, R. Chandra: *Bull. Mater. Sci.* 32 (2009) 117. DOI:10.1007/s12034-009-0018-8
- [21] G.M. Matenoglou, Ch.E. Lekka, L.E. Koutsokeras, G. Karras, C. Kosmidis, G.A. Evangelakis, P. Patsalas: *J. Appl. Phys.* 105 (2009) 103714. DOI:10.1063/1.3131824
- [22] G.M. Matenoglou, L.E. Koutsokeras, Ch.E. Lekka, G. Abadias, C. Kosmidis, G.A. Evangelakis, P. Patsalas: *Surf. Coat. Technol.* 204 (2009) 911. DOI:10.1016/j.surfcoat.2009.06.032
- [23] P. Hones, R. Sanjines, F. Levy: *Thin Solid Films* 332 (1998) 240. DOI:10.1016/S0040-6090(98)00992-4
- [24] M.S.R.N. Kiran, M.G. Krishna, K.A. Padmanabhan: *Appl. Surf. Sci.* 255 (2008) 1934. DOI:10.1016/j.apsusc.2008.06.122
- [25] K.A. Padmanabhan, M.G. Krishna and M.S.R.N. Kiran: *Patent WO2009069150* (2009).
- [26] K. Vasu, M.G. Krishna, K.A. Padmanabhan: *Appl. Surf. Sci.* 257 (2011) 3069. DOI:10.1016/j.apsusc.2010.10.118
- [27] K. Vasu, M.G. Krishna, K.A. Padmanabhan: *Appl. Phys. A* 108 (2012) 993. DOI:10.1007/s00339-012-7012-5

(Received August 30, 2012; accepted March 14, 2013; online since April 30, 2013)

## Bibliography

DOI 10.3139/146.110938  
*Int. J. Mater. Res.* (formerly *Z. Metallkd.*)  
 104 (2013) 9; page 879–884  
 © Carl Hanser Verlag GmbH & Co. KG  
 ISSN 1862-5282

## Correspondence address

Prof. K. A. Padmanabhan  
 School of Engineering Sciences and Technology  
 University of Hyderabad  
 Hyderabad  
 India  
 Tel: +91 (40)23134455  
 E-mail: kapse@uohyd.ernet.in  
 ananthaster@gmail.com

You will find the article and additional material by entering the document number **MK110938** on our website at [www.ijmr.de](http://www.ijmr.de)